Imaging of Vapor Plumes Produced by Matrix Assisted Laser Desorption: A Plume Sharpening Effect

A. A. Puretzky, D. B. Geohegan, G. B. Hurst, and M. V. Buchanan
Oak Ridge National Laboratory, Oak Ridge, Tennessee 37831

B. S. Luk'yanchuk
General Physics Institute, Russian Academy of Sciences, 117942 Moscow, Russia
(Received 31 December 1998)

The first gated imaging of both light matrix molecule and heavy biomolecule vapor expansion during matrix assisted laser desorption and ionization is reported, revealing a plume sharpening effect. Laser induced fluorescence imaging of dye-tagged DNase I proteins shows that these heavy molecules (30 000 Da) propagate within a very narrow angular distribution compared to that of the 3-HPA matrix (139 Da). A special solution of the gas dynamic equations is developed to describe the 3D coexpansion of heavy and light plume components.

PACS numbers: 79.20.Ds, 47.70.Nd, 82.80.Ms, 87.80.–y

Matrix assisted laser desorption and ionization (MALDI) is rapidly becoming an established commercial technique for the fast mass analysis of very heavy biomolecules (up to several hundred thousand daltons) [1,2]. Despite the speed and accuracy offered by the technique, improvements in efficiency, resolution, and reliability are necessary for MALDI to assume a leading position in genome sequencing [3] and practical applications in gene related disease diagnosis. MALDI utilizes laser evaporation of a host matrix and, in most cases, time-of-flight (TOF) mass spectrometric detection of a vaporized, ionized biomolecule [1]. However, the fundamental physics of this process is poorly understood. In particular, the mechanism of ejection, and the initial velocities of the ejecta, the extent of collisions between the matrix vapor and biomolecules during expansion, the times to establish final velocity distributions, and the mechanism(s) of ionization are all open questions. Understanding how MALDI vapor plumes form and propagate is essential for the enhancement of ion yields and resolutions of TOF mass spectrometers. This is especially true considering the recently developed pulsed-delayed-extraction technique [4]. Very little has been done to study 2D dynamics of MALDI plumes under actual mass spectrometric experimental conditions. Heise and Yeung [5] have used a scanned cw-Ar^+ laser and transient imaging technique, and Preisler and Yeung [6] have employed absorbance detection to image the plumes of both matrix and analyte molecules. However these studies were carried out at atmospheric pressure, where the nascent expansion of the ejected species was radically changed by gas dynamic interactions with the ambient air. The mass spectrometric measurements of Beavis and Chait [7] and Zhang and Chait [8] showed that embedded molecules are ejected with velocity $\sim 7.5 \times 10^4$ cm/s in the axial direction regardless of the mass (1000–15 600 Da) and are characterized by strongly forward-peaked angular distributions. Recently we reported the first gated laser induced fluorescence (LIF) images, optical absorption and ion probe measurements of 3-hydroxypicolinic acid (3-HPA) matrix vapor plume [9].

In this Letter we report the results of the first gated LIF imaging of the expansion of both matrix and analyte molecules during MALDI in vacuum. The expansion dynamics of the small concentration of heavy biomolecules demonstrates a very narrow angular distribution which becomes sharper for extended times compared to that of the matrix molecules. A special solution of the gas dynamic equations is developed to describe the generalized 3D expansion of heavy and/or light two-component plumes.

In these experiments, MALDI samples were prepared by mixing a small number fraction ($\sim 10^{-4}$) of heavy dye-tagged protein molecules [Deoxyribonuclease I (DNase I), 29 062 Da, labeled with an average of three covalently attached tetramethylrhodamine (TMR) dye molecules, 444 Da] in a solution of light matrix (3-HPA, molecular weight, 139 Da). This solution was deposited onto a 1-in.-diam stainless steel substrate and allowed to crystallize via the dried-droplet technique [10]. Plumes of desorbed matrix and protein molecules were generated by irradiating the matrix crystals containing the dye-tagged protein in vacuum (5×10^{-6} Torr) with a pulse of 248 nm light from a KrF laser (30° incidence angle, 50 mJ/cm^2 energy density) as shown in Fig. 1(a). For imaging of matrix and dye-tagged protein molecules propagating into vacuum, a pulse of light from an excitation laser was introduced above the target surface at different time delays following the desorption laser pulse [see Fig. 1(a)]. Fluorescence from the excited molecules was photographed with a gated, intensified charge coupled device (ICCD) array [11] camera system (100 ns gate width, synchronous with the excitation laser pulse). For imaging of 3-HPA matrix molecules in the gas phase, the strong absorption band at 300 nm was pumped with the pulsed output of a XeCl laser (308 nm, 26 ns FWHM, 25 mJ/cm^2) yielding luminescence at 430 nm [9]. For

 0031-9007/99/83(2)/444(4)$15.00

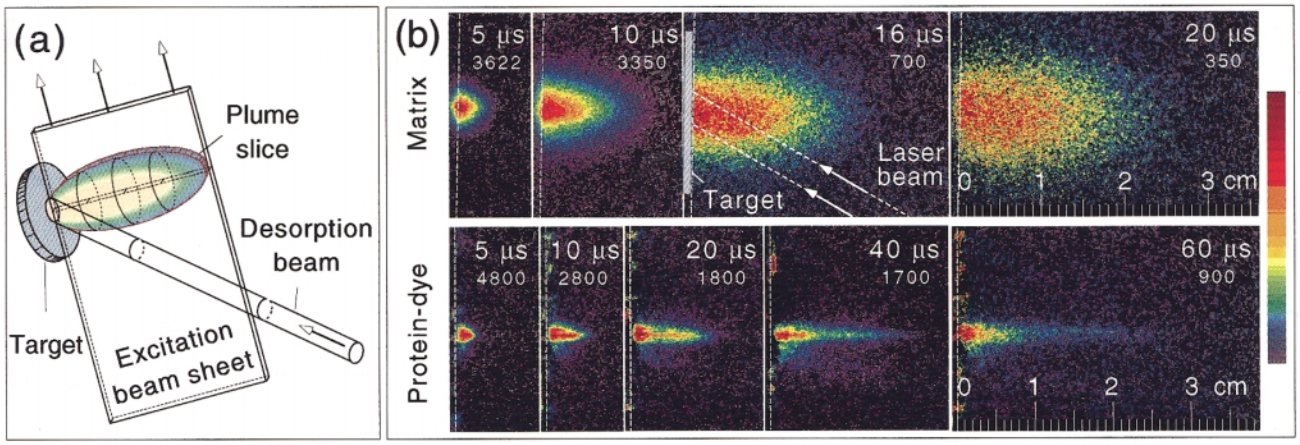

FIG. 1 (color). (a) Schematic of MALDI plume irradiation geometry. Desorption is generated by a KrF-laser beam (3.1×3.6 mm^2 elliptical beam spot). LIF excitation utilizes a sheet beam from a second laser fired at variable time delay after the desorption laser pulse. (b) ICCD images (100 ns gate width, opened 50 ns prior to the LIF laser pulse) of LIF from matrix and dye-tagged protein molecules. Each image represents a different desorption event. Time delays after desorption and the maximum intensity (red, see palette) of each image are listed. Dashed lines show the target position. (Upper row) LIF images of 3-HPA matrix vapor plume (*excitation*: 308-nm XeCl, 1.6×35.0 mm^2 rectangular beam spot); (lower row) LIF images of TMR-dye labeled DNase I protein (3.1×10^{-5} M) embedded within 3-HPA matrix and desorbed with a KrF laser (*excitation*: 532-nm second harmonic of Nd:YAG laser, 0.3×35 mm^2 beam spot). A 550-nm long-pass filter was used to cut off 532-nm scattered laser light.

the dye-tagged protein, the second harmonic of a pulsed Nd:YAG laser (532-nm, 8 ns FWHM, 40 mJ/cm^2) was used to pump the broad absorption band at 555 nm, yielding luminescence of 580 nm.

Figure 1(b) shows images which reveal, for the first time, the separate propagation dynamics of the plumes of matrix and protein molecules. Each image is the result of a single laser shot. The matrix plume exhibits a characteristic half-elliptical shape and expands rapidly in both forward and lateral directions. The dye-tagged protein plume [Fig. 1(b)] has a completely different shape; it propagates in very narrow jets which appear to originate from different microcrystals. Figure 2 helps explain the image processing procedure we used to derive the experimental parameters which were used to characterize the matrix and the protein plumes. Contour plots and line profiles along the axial (Z) and radial (R) directions are shown for two of the images of Fig. 1(b). We used the elliptical plume shape predicted by the theory of isentropic plume expansion [12] to fit the 2D-plume profiles. The inset in Fig. 2(a) demonstrates the results of this fit, where the half-ellipse curve fits the 5% contour of the maximum emission intensity of the matrix plume measured at 10 μs [see also Fig. 1(b)]. The other contours shown in this inset represent different emission intensities and demonstrate that the matrix plume maintains the nearly elliptical 2D shape. The intensity of the laser induced fluorescence from the matrix is proportional to the plume density, $\rho(x_i)$, which can be described by a Gaussian profile, $\rho \propto \exp[-\frac{1}{\gamma-1}(\sum_{i=1}^{3} \frac{x_i^2}{X_i^2})]$, in the case of the small adiabatic exponent, $\gamma = c_p/c_v$, where $x_1 = x_2 = r$ and $x_3 = z$ are the plume coordinates in the axial and the radial directions, respectively, and $X_1 = X_2 = R$ and $X_3 = Z$ are the plume leading edge positions [12]. Figure 2 shows the axial (a) and the radial (b) matrix emission intensity profiles and their Gaussian fit. These profiles were used to derive the adiabatic parameter γ by replotting these curves in the coordinates [log(emission intensity), z^2 or r^2]. At

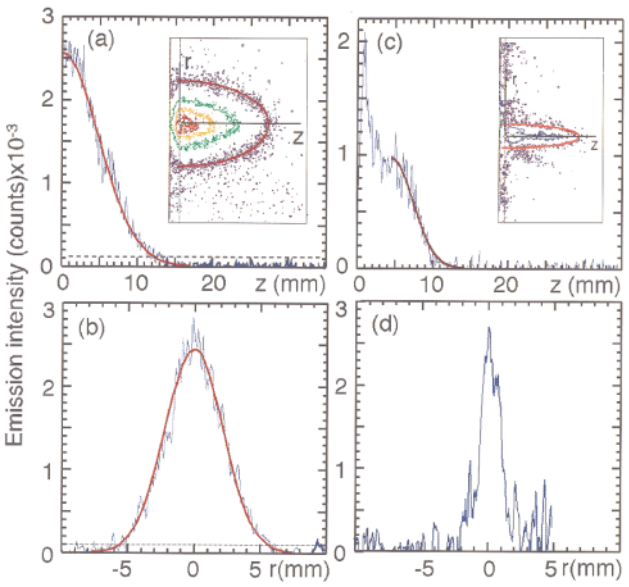

FIG. 2 (color). The axial (a) and the radial (b) line profiles of the matrix plume measured at 10 μs and the dye-protein plume [(c),(d)] obtained at 20 μs. The red lines are the result of Gaussian fits. The insets show the contour plots of the 10-μs image of the matrix (*contour emission intensities*: 128, 750, 1500, and 2250 counts) and the 20-μs image of the dye-protein (*contour emission intensities*: 125, 700, and 2000 counts) plumes. The contours corresponding to the 5% of the maximum emission intensity are fitted with the elliptical curves shown by the solid lines in these insets.

the beginning of the plume expansion γ is equal to 1.1 and increases with time ($\gamma = 1.2$ at 20 μs) indicating cooling of the matrix molecules during expansion. The leading-edge positions of the matrix plume, R and Z, were defined at the points where the Gaussian curve fit crosses the 5% maximum intensity level shown by the dotted lines in Figs. 2(a) and 2(b). The overall shape and leading-edge positions of the protein plume in the R and Z directions were determined in nearly the same way. However, as shown in Figs. 2(c) and 2(d), the protein plume has a more complicated structure, i.e., double maxima in the axial direction and non-Gaussian radial profiles. Nevertheless, the overall plume shape (5% maximum intensity contour) is well represented by a half-elliptical curve [see inset in Fig. 2(c)]. Figure 3 summarizes the positions for the leading edges of both matrix and protein plumes measured in the axial and the radial directions at different time delays. One can see that the matrix and the protein plumes propagate with comparable velocities in the axial directions, but the radial velocities are much different. The protein plume expands very slowly in the radial direction compared to the matrix plume.

The expansion of the light matrix plume is governed by the pressure gradients, $\nabla P_{\ell Z} \approx P_\ell / Z_0$, $\nabla P_{\ell R} \approx P_\ell / R_0$, in the radial and the axial directions and can be described by the gas dynamics equations [12]. The pressure at the target surface, P_ℓ, drops rapidly as the matrix vapor expands. This light material quickly enters the inertial collisionless regime after a transition time ~ 10 μs. The gas dynamics equations can be reduced to a set of ordinary differential equations for the coordinates of the plume edges (here the plume is considered as a 3D elliptical shape and the index, ℓ, refers to the light matrix) [12],

$$\ddot{X}_{i\ell} = -\frac{\partial U}{\partial X_{i\ell}}, \qquad U = \frac{(5\gamma_\ell - 3)E_\ell}{(\gamma_\ell - 1)M_\ell}\left[\prod_{i=1}^{3}\frac{X_{i\ell 0}}{X_{i\ell}}\right]^{\gamma_\ell - 1} \tag{1}$$

where $X_{i\ell 0}$ are the initial coordinates, M_ℓ is the total evaporated mass, and E_ℓ is the initial energy of the plume. The initial conditions are

$$\begin{aligned} X_{1\ell}(0) = X_{2\ell}(0) = R_0, \qquad & X_{3\ell}(0) = Z_{\ell 0}, \\ \dot{X}_{1\ell}(0) = \dot{X}_{2\ell}(0) = 0, \qquad & \dot{X}_{3\ell}(0) = v_{z0}. \end{aligned} \tag{2}$$

Although curve fits such as Figs. 2(a) and 2(b) demonstrated that γ_ℓ changes during the expansion, the value $\gamma_\ell = 1.2$ determined for the terminal region of the expansion was used as the constant in Eq. (1). The parameter $R_0 = 1.8$ mm is the radius of the laser spot. Three other parameters $Z_{\ell 0}$, v_{z0}, and $v_\ell = (E_\ell / M_\ell)^{1/2}$ were found from the best-fit procedure, which yields $Z_{\ell 0} \approx 100$ μm, $v_{z0} \approx 6 \times 10^4$ cm/s, and $v_\ell \approx 3.3 \times 10^4$ cm/s. The solution of Eqs. (1) and (2) approximates the matrix expansion quite well [see Fig. 3(a)].

For the heavy protein plume, the partial pressure, P_h, is much smaller compared to P_ℓ due to the relatively small initial concentration of the heavy molecules ($P_h / P_\ell \sim 10^{-4}$). Therefore one can neglect the pressure gradients within the heavy plume initially. Apart from the initial velocity provided by the desorption process, the only subsequent mechanism which drives the heavy molecules is collisions with the light matrix vapor. These collisions can be modeled by the introduction of the frictional force. The velocity of the heavy plume $\mathbf{u}$ ($\mathbf{v}$ is velocity of the light vapor) is defined by the following equation:

$$\frac{\partial \mathbf{u}}{\partial t} + (\mathbf{u}\nabla)\mathbf{u} = \beta(\mathbf{v} - \mathbf{u}), \qquad \beta = \frac{m}{M}\nu_c, \tag{3}$$

where m and M are masses of the matrix and the protein molecules, ν_c is the collision frequency, $\beta = \text{const}$, and consider a special solution of the problem, when the heavy plume velocities are linear functions of coordinates [12]. Then the Euler's equation (3) yields the set of equations for the propagation of the protein plume edge,

$$\ddot{X}_{ih} = \beta\left(\frac{X_{ih}}{X_{i\ell}}\dot{X}_{i\ell} - \dot{X}_{ih}\right). \tag{4}$$

This set of equations was solved with analogous boundary conditions to Eq. (2). The best fit to the data is shown in Fig. 3(b). The initial radius of the protein plume found from the smooth interpolation of the R profiles to zero time delay, $t = 0$, yields $X_{1h0} = X_{2h0} = 0.1$ cm $= R_0/1.8$. To avoid the influence of the initial asymmetry onto the sharpening effect, we put $X_{3h0} = Z_{\ell 0}/1.8$. Furthermore, the two parameters $\beta \approx 3 \times 10^4$ s^{-1} and $u_{z0} \approx 5.5 \times 10^4$ cm/s for the protein plume propagation were also determined. Separate fitting of the

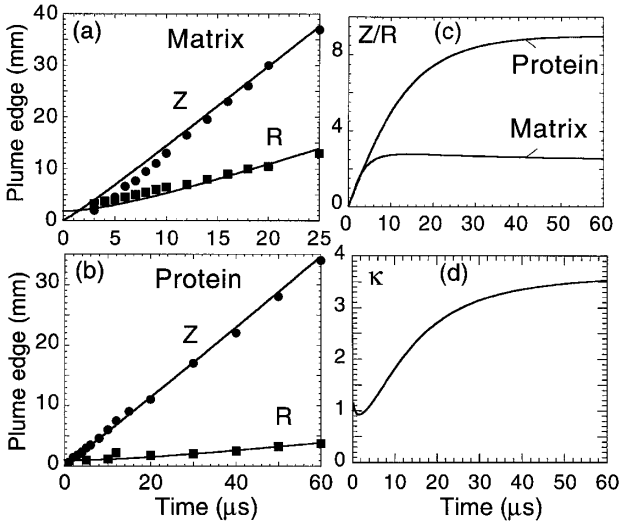

FIG. 3. The experimental (points) and the calculated (solid curves) positions of the leading edges of (a) matrix and (b) dye-tagged protein vapor plumes in the axial, Z, and the radial, R, directions at different time delays after desorption laser pulse, and (c) the calculated ratio, Z/R. (d) Time evolution of the sharpening parameter, κ.

experimental $R(t)$, $Z(t)$ for the matrix and the protein plumes yielded $u_{z0} \approx v_{z0}$, i.e., the initial velocities of the emitted molecules are practically independent of their masses. This agrees with the measurements of Beavis and Chait [7]. The probable mechanisms of these similar initial velocities are (a) the desorption from a thermally expanding surface, $v_{z0} \approx c_s \approx 10^5$ cm/s, where c_s is the characteristic sound velocity in the solid matrix, or (b) the "gun effect" [13] [$v_{z0} \approx (c_v \Delta T)^{1/2}$, $\Delta T \sim 10^3$ K, $c_v \sim 1$ J/gK, and $v_{z0} \approx 10^5$ cm/s, where ΔT is the characteristic initial temperature of the vapor due to laser heating.] Figure 3(a) and 3(b) show that this model adequately describes the overall expansion of the matrix and the protein plumes and correctly represents the measured asymmetries in the expansion velocities. Figure 3(c) shows the temporal evolution of the relative dimensions of the plume (Z/R) of both the matrix and the protein obtained from the theoretical fits shown in Figs. 3(a) and 3(b). The images [Fig. 1(b)] clearly show that after $\sim$10 μs the relative dimensions of the light matrix plume remain the same, i.e., $Z_\ell/R_\ell = \text{const}$. This is not the case for the heavy protein plume which continues to sharpen (increasing Z_h/R_h) for a much longer time, 30–40 μs, which can be defined by a characteristic transition time $\sim 1/\beta$. We apply the term "sharpening effect" to describe the ever-narrowing angular distribution of the heavy molecules relative to the light matrix molecules and introduce the sharpening parameter, $\kappa = Z_h R_\ell / Z_\ell R_h$, to characterize this effect. The sharpening parameter, κ, continues to increase during the transition time and then satures [Fig. 3(d)].

In conclusion, this first gated LIF imaging of laser-desorbed biomolecules and matrix vapors reveals that the small concentration of heavy biomolecules propagate within a very narrow angular distribution which continues to sharpen over extended times after laser desorption. The "sharpening" of the heavy biomolecule plume results from the lack of radial frictional interaction with the light matrix vapor due to the poor spatial overlap of the two plumes during the period of matrix radial expansion.

This research was sponsored by the LDRD Program at Oak Ridge National Laboratory, managed by Lockheed Martin Energy Research Corporation, for the U.S. Department of Energy, under Contract No. DE-AC05-96OR22464. B. S. L. was supported by RBRF (Grant No. 98-02-16104).

[1] M. Karas and F. Hillenkamp, Anal. Chem. **60**, 2299 (1988).
[2] S. Berkenkamp, F. Kirpekar, and F. Hillenkamp, Science **281**, 260 (1998).
[3] D. J. Fu, K. Tang, A. Braun, B. Darnhover-Demar, D. P. Little, M. J. O'Donnell, C. R. Cantor, and H. Koster, Nature Biotechnol. **16**, 381 (1998).
[4] P. Juhasz, M. T. Roskey, I. P. Smirnov, L. A. Haff, M. L. Vestal, and S. A. Martin, Anal. Chem. **68**, 941 (1996).
[5] T. W. Heise and E. S. Yeung, Anal. Chem. **66**, 355 (1994).
[6] J. Preisler and E. S. Yeung, Appl. Spectrosc. **49**, 1826 (1995).
[7] R. C. Beavis and B. T. Chait, Chem. Phys. Lett. **181**, 479 (1991).
[8] W. Zhang and B. T. Chait, Int. J. Mass Spectrom. Ion Process. **160**, 259 (1997).
[9] A. A. Puretzky and D. B. Geohegan, Chem. Phys. Lett. **286**, 425 (1998).
[10] The matrix preparation procedure is described in Ref. [9]. The dye-tagged protein (DNase I/TMR dye) samples were prepared as 3×10^{-5} mol/l deionized water solutions. A 100-μl volume each of the protein and the matrix (0.3 mol/l) solutions was mixed together and placed on a stainless steel disk to crystallize.
[11] Gated imaging was performed with the ICCD lens-coupled camera system (Princeton Instruments, 576 $\times$ 384 pixels, 12.7 $\times$ 8.4 mm^2 array, 22 $\times$ 22 μm^2 pixel size, one image per laser shot) with variable gain and gate width (5 ns minimum) and a spectral range from 200 to 820 nm.
[12] S. I. Anisimov, D. Bauerle, and B. S. Luk'yanchuk, Phys. Rev. B **48**, 12 076 (1993).
[13] B. Branen, K. G. Casey, and R. Kelly, Nucl. Instrum. Methods Phys. Res., Sect. B **58**, 463 (1991).